AD-A168 972 AN ANALYSIS OF SHEAR BAND DEVELOPMENT INCORPORATING HEAT CONDUCTION(U) BROWN UNIV PROVIDENCE RI DIV OF EEGINEERING J LEMONDS ET AL. MAY 86 ARO-22306.5-EG 1/1

UNCLASSIFIED DAAG29-85-K-0003 F/G 20/13 NL

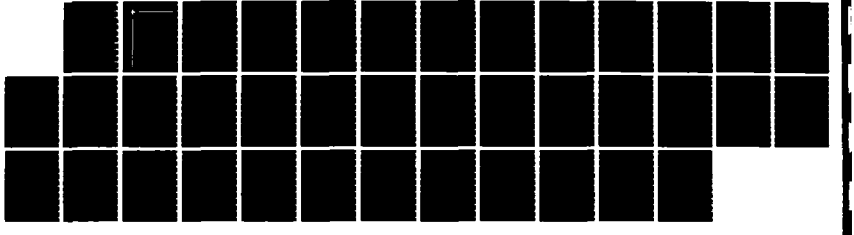

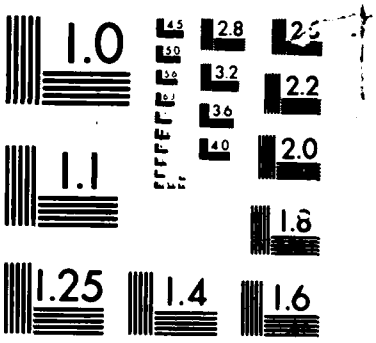
1.0
1.1
1.25
1.4
1.6
1.8
2.0
2.2
2.8
3.2
3.6
4.0

Brown University
DIVISION OF ENGINEERING
PROVIDENCE, R.I. 02912

AN ANALYSIS OF SHEAR BAND DEVELOPMENT INCORPORATING HEAT CONDUCTION

by

J. LeMonds and A. Needleman
Division of Engineering
Brown University
Providence, R.I. 02912

AN ANALYSIS OF SHEAR BAND DEVELOPMENT INCORPORATING HEAT CONDUCTION

by

J. LcMonds and A. Needleman
Division of Engineering
Brown University
Providence, R.I. 02912

Army Research Office Report
No. DAAG 29-85-K-0003/5

May, 1986

UNCLASSIFIED

SECURITY CLASSIFICATION OF THIS PAGE (When Data Entered)

AD-A168 972

REPORT DOCUMENTATION PAGE		READ INSTRUCTIONS BEFORE COMPLETING FORM
1. REPORT NUMBER ARO 22366.5-EG	2. GOVT ACCESSION NO. N/A	3. RECIPIENT'S CATALOG NUMBER N/A
4. TITLE (and Subtitle) "An Analysis of Shear Band Development Incorporating Heat Conduction"		5. TYPE OF REPORT & PERIOD COVERED Technical 6. PERFORMING ORG. REPORT NUMBER
7. AUTHOR(s) J. LeMonds and A. Needleman		8. CONTRACT OR GRANT NUMBER(s) DAAG 29-85-K-0003
9. PERFORMING ORGANIZATION NAME AND ADDRESS Division of Engineering Brown University Providence, RI 02912		10. PROGRAM ELEMENT, PROJECT, TASK AREA & WORK UNIT NUMBERS N/A
11. CONTROLLING OFFICE NAME AND ADDRESS U. S. Army Research Office Post Office Box 12211 Research Triangle Park, NC 27709		12. REPORT DATE May, 1986 13. NUMBER OF PAGES 33
14. MONITORING AGENCY NAME & ADDRESS(if different from Controlling Office)		15. SECURITY CLASS. (of this report) Unclassified 15a. DECLASSIFICATION/DOWNGRADING SCHEDULE

16. DISTRIBUTION STATEMENT (of this Report)

Approved for public release; distribution unlimited.

17. DISTRIBUTION STATEMENT (of the abstract entered in Block 20, if different from Report)

NA

18. SUPPLEMENTARY NOTES

The view, opinions, and/or findings contained in this report are those of the author(s) and should not be construed as an official Department of the Army position, policy, or decision, unless so designated by other documentation.

19. KEY WORDS (Continue on reverse side if necessary and identify by block number)

Shear Bands
Shear Localization
Thermoplastic Instability
Thermal Softening

20. ABSTRACT (Continue on reverse side if necessary and identify by block number)

We incorporate the effects of material temperature sensitivity and heat conduction into an infinite band type analysis of shear localization. Full account is taken of finite geometry changes, but inertial effects are neglected. An energy balance is written between homogeneously deforming bands in a manner that models conditions in our recent finite element study of shear band development from internal inhomogeneities in a solid subject to plane strain compression. The band analysis requires specification of an imperfection amplitude and a length scale over which heat conduction effects are significant. These are chosen to

DD FORM 1 JAN 73 1473 EDITION OF 1 NOV 65 IS OBSOLETE

UNCLASSIFIED

AN ANALYSIS OF SHEAR BAND DEVELOPMENT INCORPORATING HEAT CONDUCTION

by

J. LeMonds

and

A. Needleman
Division of Engineering
Brown University
Providence, RI 02912 U.S.A.

ABSTRACT

We incorporate the effects of material temperature sensitivity and heat conduction into an infinite band type analysis of shear localization. Full account is taken of finite geometry changes, but inertial effects are neglected. An energy balance is written between homogeneously deforming bands in a manner that models conditions in our recent finite element study of shear band development from internal inhomogeneities in a solid subject to plane strain compression. The band analysis requires specification of an imperfection amplitude and a length scale over which heat conduction effects are significant. These are chosen to match results of a finite element analysis. The predictions of the simple band analysis and the results of full finite element calculations are then compared for a wide range of material properties for both isotropic and kinematic hardening characterizations of the flow potential surface. The predicted dependence of the onset of localization on material properties such as strain hardening and strain rate sensitivity is the same for both types of analysis.

1. INTRODUCTION

Shear bands frequently accompany the large plastic straining of materials. The large localized strains in a shear band often precipitate fracture. When shear bands do not lead to fracture the localized shearing greatly affects subsequent plastic deformation. Hence, shear bands have a dual significance: as a precursor to fracture and as a mechanism for large strain plastic deformation. In metals subject to high rates of loading, shear bands can form as the result of a thermomechanical instability. The same metal may also undergo shear localization at very low strain rates, where thermal effects are negligible, with some other mechanism causing the localization.

In this paper, we present a method for predicting the onset of shear localization in rate and temperature dependent solids. Localization is regarded as an instability which develops as the result of the growth of an initial inhomogeneity in a narrow plane (the imperfection band) of an otherwise homogeneous material. We carry out our analysis withi a framework that regards localization as a material instability (Hill [1], Thomas [2], Mandel [3], Rice [4]), which has been used to analyze the influence of a variety of constitutive features on localization, e.g. Rice [4], Hill and Hutchinson [5], and Needleman and Rice [6]. The general framework for imperfection-based localization studies for time independent solids has been presented by Rice [4], which follows the shear band bifurcation methodology inherent in Marciniak and Kuczynski's [7] analysis of localized necking in thin sheets. Studies of localization along these lines have been carried out by Hutchinson and Tvergaard [8] and Saje, Pan and Needleman [9]. The effects

of material strain rate sensitivity have been included by Pan, Saje and Needleman [10].

The present analysis for localization builds upon the existing framework for rate dependent solids in [10] by incorporating temperature sensitivity into the formulation. Attention is focused on the response in the imperfection band and in a thin strip of material at a characteristic distance from it. The conditions under which a highly localized pattern of deformation in the imperfection band can emerge relative to an imposed homogeneous deformation in the material strip are sought.

The onset of localization depends critically on the details of the assumed constitutive law. It is well known that yield surface curvature plays an important role in the localization process. The classical elastic-plastic solid with a smooth yield surface is quite resistant to localization, Rudnicki and Rice [11]. However, for a kinematically hardening solid with a smooth yield surface, localization is possible at achievable strain levels in the three-dimensional shear localization context, Hutchinson and Tvergaard [8]. This effect has also been observed in the plane stress sheet necking context, Tvergaard [12] and Needleman and Tvergaard [13].

Analyses are performed using a viscoplasticity theory which, in the rate independent limit, corresponds to J_2 flow theory with combined isotropic and kinematic hardening. The formulation incorporates the effects of thermal softening, strain hardening, strain rate sensitivity and heat conduction. The momentum and energy balance equations are coupled via the temperature dependent flow stress and the internal heat generation resulting from plastic deformation, and are solved simultaneously.

Full account is taken of finite geometry changes, but inertial effects are neglected. Attention is confined to a range of strain rates, from say 10^{-3} sec^{-1} to

10^3 sec^{-1}, where material rate sensitivity is the main time effect and higher strain rates where inertial effects play an important role are excluded from consideration.

2. CONDITION FOR LOCALIZATION

An infinite planar solid which contains a thin planar imperfection band is shown in Fig. 1. The imperfection band is denoted by the region labelled 'b', and a thin strip of the surrounding material located at a distance ℓ from the imperfection band is labelled 's'. The unit normal vector to both the imperfection band and the material strip, denoted by ν, is initially oriented at an angle ψ_0 from the compression axis. The width of both regions is denoted by w, and is assumed to be sufficiently small so that the properties and fields in them may be considered to be homogeneous. Material properties and field quantities in these regions are identified with a superscript or subscript 'b' or 's'.

The reference configuration for the Lagrangian formulation corresponds to the initial unstressed state with the material points identified by the Cartesian coordinates x^i. In the current deformed state, the material points are at $x^i + u^i$ where u^i are the displacement components, and $\mathbf{F} = \mathbf{I} + \partial \mathbf{u}/\partial \mathbf{x}$.

The solid is deformed quasi-statically to give the deformation rate $\dot{\mathbf{F}}^s$ in the material strip. As a result of the initial imperfection, the current value of the field quantities inside the imperfection band will generally differ from those outside it. The conditions of compatability, equilibrium and balance of energy must be satisfied.

The requirement of continuity of the velocity field takes the form (Rice [4])

$$\dot{F}^b_{ij} = \dot{F}^s_{ij} + \dot{q}_i \nu_j \tag{2.1}$$

where $(\dot{})$ denotes the material time derivative and ν is the unit normal to the imperfection band in the undeformed state. The tensor $\mathbf{q}$ represents the current deformation non-uniformity which has accumulated as a result of the initial imperfection.

The condition of incremental equilibrium between the two regions requires that

$$(\dot{n}_b^{ij} - \dot{n}_s^{ij})\, \nu_i = 0 \tag{2.2}$$

where n^{ij} are the contravariant components of the nominal stress tensor. It is assumed that the stress rate in (2.2) is expressible in the form

$$\dot{n}^{ij} = K^{ijk\ell}\, \dot{F}_{\ell k} + \dot{A}^{ij} \ . \tag{2.3}$$

The moduli $K^{ijk\ell}$ and $\dot{A}^{ij}$ are rate and temperature dependent.

Combining (2.1) through (2.3) yields

$$K_b^{ijk\ell}\, \nu_i \nu_k \dot{q}_\ell = (K_s^{ijk\ell} - K_b^{ijk\ell})\, \dot{F}_{\ell k}^{s}\, \nu_i + (\dot{A}_s^{ij} - \dot{A}_b^{ij})\, \nu_i \ , \tag{2.4}$$

which is the evolution equation for q.

Heat conduction effects are modelled assuming that the time rate of change of energy in the imperfection band due to conduction is proportional to the temperature gradient $(T_b - T_s)/\ell$. Accordingly, energy balance between the two regions results in evolution equations for T_s and T_b, given by

$$\rho\, c_p\, w \dot{T}_s = \frac{k}{\ell}(T_b - T_s) + \chi\, w\, \tau^s : d_s^p \tag{2.5}$$

$$\rho\, c_p\, w \dot{T}_b = -\frac{2k}{\ell}(T_b - T_s) + \chi\, w\, \tau^b : d_b^p \ . \tag{2.6}$$

In the equations above, ρ is the mass density, c_p is the specific heat at constant pressure, k is the thermal conductivity, τ is the Kirchhoff stress tensor, and d^p is the plastic part of the rate of deformation tensor d, which is the symmetric part of $\dot{F}\, F^{-1}$. Heat flowing out of the imperfection band flows to either side of it; hence the factor of two in (2.6). The fraction of plastic stress work which is

converted to heat is denoted by χ, and is typically in the range of 0.85 to 0.95 for ductile metals (Taylor and Quinney [14]).

The heat transfer condition incorporated in (2.5) and (2.6) is taken to model the behavior in our recent finite element study of shear localization [15] from a doubly periodic array of internal inhomogeneities. In those calculations heat conduction was accounted for within each cell surrounding an inhomogeneity, but there was no heat flux across cell boundaries.

In a planar analysis, (2.4) through (2.6) constitute a system of four differential equations which govern the state of the system. Localization occurs when one of the components of the rate of deformation tensor within the imperfection band becomes infinite. In the rate independent limit, $\dot{A} = 0$, and localization occurs when the determinant of $(K_b^{ijk\ell}\, \nu_i \nu_k)$ vanishes (Rice [4]).

Two dimensionless groups characterize the thermal response,

$$\bar{\xi} = \frac{k}{\rho c_p\, w\ell \dot{\epsilon}_n}, \qquad \eta = \frac{\chi\, \sigma_o}{\rho c_p T_o}. \tag{2.7}$$

Here, $\dot{\epsilon}_n$ is a reference strain rate, T_o is a reference temperature, and σ_o is a reference stress. Uniform temperature behavior results as $\bar{\xi}$ approaches infinity, and adiabatic conditions are obtained as $\bar{\xi}$ approaches zero. The characteristic length $(k/\rho c_p\, \dot{\epsilon}_n)^{1/2}$ governs the extent over which the effects of heat conduction are significant. We note that the length scale $(w\ell)^{1/2}$ entering the definition of non-dimensional parameter $\bar{\xi}$ is different from the length scale used to define a similar non-dimensional parameter in our finite element study of shear localization in [15]. The rate of internal heat dissipation is controlled by the parameter η.

3. CONSTITUTIVE RELATIONS

The flow potential surfaces are taken to be concentric cylinders centered about a stress state α in stress space. The radius of the flow potential surface is denoted by σ_F and is given by

$$\sigma_F = \left[\frac{3}{2}\,\bar{\mathbf{S}}:\bar{\mathbf{S}}\right]^{1/2} \tag{3.1}$$

where $\bar{\mathbf{S}} = \mathbf{S}-\alpha$ The tensor $\mathbf{S}$ is the Kirchhoff stress deviator, given by $\mathbf{S} = \tau - 1/3\tau : \mathbf{I}$, where $\mathbf{I}$ is the identity tensor. Here, the kinematic and isotropic hardening plastic flow rules are based on Kirchhoff stress rather than on Cauchy stress. As long as elastic strains remain small, there is little difference between the two formulations.

The rate of deformation tensor is expressed as the sum of elastic and plastic parts by

$$\mathbf{d} = \mathbf{d}^e + \mathbf{d}^p \,. \tag{3.2}$$

The elastic part is given by

$$\mathbf{d}^e = \mathbf{L}^{-1} : \overset{\triangle}{\tau} \tag{3.3}$$

where $\overset{\triangle}{\tau}$ is the Jaumann rate of Kirchhoff stress and $\mathbf{L}$ is a fourth order tensor representing the elastic stiffness of the material. The plastic part of the rate of deformation tensor is given by

$$\mathbf{d}^p = \frac{3\dot{\bar{\epsilon}}}{2\sigma_F}\,\bar{\mathbf{S}} \,. \tag{3.4}$$

Here, $\dot{\bar{\epsilon}}$ is specified by the power law relation

$$\dot{\bar{\epsilon}} = \dot{\epsilon}_0 \left[\frac{\sigma_F}{[1-\beta(T-T_0)]h(\bar{\epsilon})}\right]^{1/m} \tag{3.5}$$

where $\dot{\epsilon}_0$ is a reference strain rate, T_0 is a reference temperature, m is the strain rate hardening exponent and β specifies the thermal softening characteristics of

the material. This assumed linear temperature dependence is representative of carbon steels in the range 0 - 500°C, e.g. Staker [16], although at elevated temperatures the flow stress is generally a non-linear function of temperature.

We employ combined isotropic and kinematic hardening, Goel and Malvern [17], with $h(\bar{\epsilon})$ and the evolution equation for α given by

$$h(\bar{\epsilon}) = \lambda \sigma_0[1 + \bar{\epsilon}/\epsilon_0]^N + (1-\lambda) \sigma_0 \tag{3.6}$$

$$\overset{\nabla}{\alpha} = \frac{2}{3}(1 - \lambda)b\, \mathbf{d}^p \tag{3.7}$$

where

$$b = \left[\frac{\dot{\bar{\epsilon}}}{\dot{\epsilon}_0}\right]^m [1 - \beta(T-T_0)] \; N \frac{\sigma_0}{\epsilon_0}[1 + \bar{\epsilon}/\epsilon_0]^{N-1} \tag{3.8}$$

Here, σ_0 is a reference stress, ϵ_0 is a reference strain, N is the strain hardening exponent and λ is a constant ranging between zero and unity. Purely isotropic hardening corresponds to $\lambda = 1$, while purely kinematic hardening is given by $\lambda = 0$. The evolution equation for b, (3.8), is taken so that at constant strain rate and temperature, the response for proportional loading is independent of whether the change in flow potential surface is described by isotropic hardening or by kinematic hardening, see Needleman and Tvergaard [13].

An expression for the Jaumann rate of Kirchhoff stress is obtained in terms of rate quantities by combining (3.2) through (3.4),

$$\overset{\nabla}{\mathbf{t}} = \mathbf{L} : \mathbf{d} - \frac{3\dot{\bar{\epsilon}}}{2\sigma_F} \mathbf{L} : \bar{\mathbf{S}} \tag{3.9}$$

Although there is no explicit yielding in this formulation, for small m there is an effective yield point in that plastic strain rates are very small when the numerator is less than the denominator in (3.5).

4. FINITE ELEMENT IMPLEMENTATION

4.1 Rate Tangent Modulus

In order to increase the stable step size over that of an explicit Euler time integration scheme, Peirce et al. [18] employ a formulation which results in a tangent modulus type method for solving the governing rate equations. The method is explicit in that no iterations are required. In this method the effective uniaxial plastic strain rate $\dot{\bar{\epsilon}}$ within an increment is expressed as a linear combination of its rates at times t and t + Δt by

$$\dot{\bar{\epsilon}} = (1 - \theta)\dot{\bar{\epsilon}}_t + \theta\dot{\bar{\epsilon}}_{t+\Delta t} \tag{4.1}$$

where θ is a parameter ranging from zero to unity. The plastic strain rate at time t + Δt is approximated by

$$\dot{\bar{\epsilon}}_{t+\Delta t} = \dot{\bar{\epsilon}}_t + \left[\left.\frac{\partial \dot{\bar{\epsilon}}}{\partial \sigma_F}\right|_t \dot{\sigma}_F + \left.\frac{\partial \dot{\bar{\epsilon}}}{\partial \bar{\epsilon}}\right|_t \dot{\bar{\epsilon}} + \left.\frac{\partial \dot{\bar{\epsilon}}}{\partial T}\right|_t \dot{T} \right] \Delta t \, . \tag{4.2}$$

An expression for $\dot{\sigma}_F$ is obtained by *differentiating* (3.1) and using (3.7) and (3.9),

$$\dot{\sigma}_F = \frac{3}{2\sigma_F} \mathbf{L} : \bar{\mathbf{S}} : \mathbf{d} - [3G + (1 - \lambda)b]\dot{\bar{\epsilon}} \tag{4.3}$$

where G is the elastic shear modulus and b is given by (3.8).

Combining (4.1) through (4.3) and solving for $\dot{\bar{\epsilon}}$ yields

$$\dot{\bar{\epsilon}} = \dot{p} + \frac{3\dot{q}}{2\sigma_F} \mathbf{L} : \bar{\mathbf{S}} : \mathbf{d} \tag{4.4}$$

where

$$\dot{p} = \frac{\dot{\bar{\epsilon}}_t}{D} \left[1 + \frac{\theta\beta\Delta t}{m[1 - \beta (T - T_0)]} \dot{T} \right] \tag{4.5}$$

$$\dot{q} = \frac{\theta\Delta t \dot{\bar{\epsilon}}_t}{D \, m \, \sigma_F} \tag{4.6}$$

$$D = 1 + \frac{\theta\Delta t \dot{\bar{\epsilon}}_t}{m} \left[\frac{3G + (1 - \lambda)b}{\sigma_F} + \frac{\lambda}{h} N \frac{\sigma_o}{\epsilon_o} (1+\bar{\epsilon}/\epsilon_o)^{N-1} \right] . \tag{4.7}$$

Substitution of (4.4) into the expression for the Jaumann rate of Kirchhoff stress given by (3.9) results in

$$\overset{\nabla}{\boldsymbol{\tau}} = \mathbf{C} : \mathbf{d} - \frac{3\dot{p}}{2\sigma_F} \mathbf{L} : \bar{\mathbf{S}} \tag{4.8}$$

where

$$\mathbf{C} = \mathbf{L} - \left[\frac{3}{2\sigma_F}\right]^2 \dot{q}\, (\mathbf{L} : \bar{\mathbf{S}})\, (\mathbf{L} : \bar{\mathbf{S}}) \tag{4.9}$$

The expression for $\overset{\nabla}{\boldsymbol{\tau}}$ given by (4.8) may be used to compute the stress rates $\dot{\tau}^{ij}$ needed for the computation of the moduli $K^{ijk\ell}$ in (2.4). The details of this computation are given by Needleman [19].

4.2 Solution of the Coupled System

Equations (2.4) through (2.6) constitute a coupled system of four differential equations which may be solved to obtain the state of the system at time $t + \Delta t$. These equations may be effectively uncoupled by introducing an estimate for the temperature rates at time $t + \theta\Delta t$, say $\dot{T}_s^e$ and $\dot{T}_b^e$, into (2.4). This is accomplished by expressing $\dot{T}$ as a quadratic function of time based on its values at the previous three points in time at which the solution has been obtained, and extrapolating to obtain $\dot{T}^e$.

Following the computation of the $\dot{q}_i$ using (2.4), the deformation gradient rate $\dot{F}_{ij}^b$ is computed from (2.1). Then the deformation gradient, stresses and internal variables in the imperfection band and the material strip are updated using a simple linear incremental updating scheme. Next, the heat generation rate $\chi\boldsymbol{\tau} : \mathbf{d}^p$ is computed in both regions, and their temperatures are calculated from (2.5) and (2.6). The stepsize is reduced if the computed and the estimated temperature rates differ by more than an allowable tolerance.

When the solution of the coupled system at time $t + \Delta t$ has been completed, this solution becomes the new current state. The procedure is then repeated to obtain the solution for the next increment.

5. NUMERICAL RESULTS

The material properties used in the calculations are chosen to be representative of a 4340 steel studied experimentally by Hartley [20], and are identical to those used in the full two-dimensional finite element calculations of shear banding by LeMonds and Needleman [15]. These properties are specified by σ_0 = 1250 MPa, E = 200,000 MPa, ν = 0.30, ϵ_0 = 0.003, N = 0.08, m = 0.01, $\dot{\epsilon}_0$ = 0.001 sec^{-1}, ρ = 7833 kg/m^3, c_p = 465 J/kg°C, k = 54 W/m°C (in the analyses involving heat conduction), β = 0.0016 per °C, and T_0 = 20°C. These values comprise a reference set of material properties which are used for comparison of critical strain predictions of the flow localization analysis to the critical strains obtained from the finite element calculations in [15]. Non-dimensional parameters which depend on σ_0 are σ_0/E = 0.00625 and η = 1.1714. The initial undeformed state is stress free and at a uniform temperature specified by T_0.

The imperfection is prescribed by specifying a value for the initial flow stress in the imperfection band which is slightly different from that in the surrounding material. We define a measure of the amplitude of the imperfection with the parameter $f = \sigma_0^b/\sigma_0^s$. Values of f less than unity are considered, implying that the material in the imperfection band is initially softer than the surrounding material.

The solid is compressed under conditions of plane strain at a constant nominal strain rate $\dot{\epsilon}_n$, with the compression axis parallel to the x^2 axis. This deformation is obtained by prescribing $\dot{F}^s_{22} = \dot{\epsilon}_n F^s_{22}$, $\dot{F}^s_{12} = \dot{F}^s_{21} = 0$, and $\dot{n}^s_{11} = 0$. The stress rate boundary condition may be used in conjunction with (2.3) to obtain

$$\dot{F}^s_{11} = - \frac{K_s^{1122} \dot{F}^s_{22} + \dot{A}_s^{11}}{K_s^{1111}} \quad . \tag{5.1}$$

The sensitivity of the critical strain to the imperfection strength f is shown in Fig. 2 for an isotropically hardening material deforming under adiabatic conditions with $\dot{\epsilon}_n/\dot{\epsilon}_o = 5\times10^5$ ($\dot{\epsilon}_n = 500$ sec^{-1}); therefore $\bar{\xi} = 0$ in (2.7) and $\lambda = 1$ in (3.6) and (3.7). The parameter ϵ_{cr} denotes the critical strain, which is the lowest value of the localization strain for all possible initial orientations of the imperfection band. The localization strain is the value of the maximum principle logarithmic strain in the material strip at the point when $\dot{\bar{\epsilon}}_b/\dot{\bar{\epsilon}}_s = 10$. The critical strain is very sensitive to the imperfection strength.

In subsequent calculations, we use a value of f = 0.9994 which yields the critical strain $\epsilon_{cr} = 0.150$ observed in the finite element calculation of the isotropically hardening solid deforming under adiabatic conditions in [15]. Although the identification of the initiation of localization in the finite element calculations is somewhat arbitrary, the strain accumulations in the band become very rapid at the indicated critical strain. The initial orientation of the band is $\psi_o = 51.7^\circ$, and its orientation at localization, given by $\tan\psi_{cr} = (F^s_{11}\tan\psi_o/F^s_{22})_{cr}$, is $\psi_{cr} = 43.1^\circ$. This result agrees well with $\psi_{cr} = 42.8^\circ$ observed in the finite element calculation.

The effect of the thermal parameter $\bar{\xi}$ on the localization strain is shown in Fig. 3 for a kinematically hardening solid deformed at $\dot{\epsilon}_n/\dot{\epsilon}_o = 5\times10^5$. The adiabatic and uniform temperature limits can be specified to within five percent error (relative to the numerical results) by $\bar{\xi} < 0.06$ and $\bar{\xi} > 175$, respectively. The critical strains at the adiabatic and uniform temperature limits are $\epsilon_{cr} = 0.170$ and 0.873, respectively, with corresponding initial band orientations of $\psi_o = 52.4^\circ$ and 76.0°.

Finite element calculations in [15] for a kinematically hardening solid with heat conduction effects were carried out for $\dot{\epsilon}_n/\dot{\epsilon}_o = 5\times10^5$, 5×10^4 and 5×10^3, which correspond to $\dot{\epsilon}_n = 500$ sec^{-1}, 50 sec^{-1} and 5 sec^{-1}. In each case,

localization occurred rapidly once a shear band initiated. The parameter $\bar{\xi}$ in (2.7) characterizes the thermal response of the solid, with $\bar{\xi} = 0$ specifying the adiabatic limit and $\bar{\xi} \to \infty$ specifying the uniform temperature limit. The value of $\bar{\xi}$ which results in localization at the critical strains at which the shear bands formed in the finite element calculations in [15] is shown in Table 1 for each of the normalized strain rates considered. These values of $\bar{\xi}$ will be used in subsequent calculations which include the effects of heat conduction.

Several finite element calculations using the numerical method in [15] have been carried out here at $\dot{\epsilon}_n/\dot{\epsilon}_o = 5\times10^5$ ($\dot{\epsilon}_n = 500$ sec^{-1}) for kinematically hardening solids with material properties which are significantly different from those used in the previous calculations. The critical strains predicted by the flow localization analysis agree quite well with the strains at which shear bands formed in the finite element calculations, as shown in Table 2.

Figures 4 through 7 depict ϵ_{cr} as a function of the material properties β, N, m and η, respectively, for a kinematically hardening solid deforming at $\dot{\epsilon}_n/\dot{\epsilon}_o = 5\times10^5$ with $\bar{\xi} = 3.37$ in (2.7). In these figures, the results of the finite element calculations reported in Table 2 are plotted with the symbol 'X'. The agreement between the predictions of the flow localization method (using a constant imperfection amplitude f = 0.9994) and the results of the finite element analyses are quite good over a range of considerable variation in the material properties.

The localization strain predicted in the temperature independent limit ($\beta \to 0$ in (3.5)) in Fig. 4 is finite, although this is not readily apparent from the figure. The localization strain in this case is very high due to the weak imperfection (f = 0.9994). A stronger imperfection will permit localization at a strain which is physically plausible. For example, $\epsilon_{cr} = 0.50$ when f = 0.991. If an isotropic hardening surface is used, then the material is so resistant to localization when

$\beta = 0$ that an imperfection specified by $f = 0.878$ is necessary in order to obtain $\epsilon_{cr} = 0.50$.

The critical strain shown as a function of the strain hardening exponent N (see (3.6)) in Fig. 5 exhibits a maximum value $\epsilon_{max} = 0.296$ at $N = 0.22$. The material stiffness and the rate of internal heat generation both increase with increasing N. Strain hardening tends to stabilize the deformation, while softening due to increased heating is destabilizing, Clifton [21]. These competing effects account for the observed maximum critical strain.

Fig. 8 shows the dependence of the localization strain on the imperfection band orientation for several values of the thermal softening parameter β in (3.5) for the case of kinematic hardening with $\bar{\xi} = 3.37$ in (2.7). The solid curves correspond to the initial band orientation, and the dashed curves correspond to the angle at localization. The imperfection band orientation at localization always falls below $\pi/4$, which is consistent with the predictions of bifurcation analyses for plane strain compression, Hutchinson and Tvergaard [8].

The jump in hydrostatic stress across the band interface is shown in Fig. 9 for several values of the strain hardening exponent N in (3.7) for a kinematically hardening solid deformed at $\dot{\epsilon}_n/\dot{\epsilon}_o = 5\times10^5$ with $\bar{\xi} = 3.37$ in (2.7). For $N > 0.17$, the hydrostatic stress in the imperfection band is less than that in the surrounding material throughout the deformation history, whereas for more lightly hardening materials the jump in hydrostatic stress is negative initially and then increases. For the case where $N = 0.05$, the maximum principal logarithmic strain is 0.224 inside the band and 0.167 outside the band when the increase in the jump in hydrostatic stress takes place. This suggests the possibility that at large accumulated shear, the hydrostatic stress in the band may become positive even though the nominal stress state is one of plane strain compression. This is of interest in regard to ductile failure

mechanisms since void growth is driven by a positive hydrostatic tension (see e.g. Rice and Tracey [22], McClintock [23]).

The effect of the mixed hardening parameter λ in (3.6) and (3.7) on the localization strain is shown in Fig. 10 for a solid compressed at $\dot{\epsilon}_n/\dot{\epsilon}_o = 5\times10^3$ ($\dot{\epsilon}_n = 5$ sec^{-1}) with $\bar{\xi} = 25.34$ in (2.7). Localization occurs at $\epsilon_{cr} = 0.554$ with $\psi_o = 69.3^\circ$ for kinematic hardening, and at $\epsilon_{cr} = 0.93$ with $\psi_o = 80.3^\circ$ for isotropic hardening. The effective stress in shear is lower for the kinematic hardening surface, and the higher curvature of that surface relative to the isotropic hardening surface results in a greater increment in shear strain for a given increment in stress. In the finite element calculation in [15] with isotropic hardening at this imposed strain rate, the solid was deformed until $\epsilon = 0.90$ without any indication of shear band formation.

6. CONCLUSIONS

The results of the present analysis indicate that shear localizaiton in rate and temperature dependent solids is strongly influenced by a variety of factors. Which factors are most influential depends on the complete description of the material - its properties and constitutive behavior - and the imposed deformation rate. For the kinematically hardening solid specified by our reference set of material parameters, and deformed in plane strain compression at $\dot{\epsilon}_n = 500$ sec^{-1}, a five-fold increase in the localization strain occurs between the adiabatic and uniform temperature limits, identifying heat conduction as the primary stabilizing effect. The main destabilizing factor in this case is thermally-induced softening: a physically plausible value of the thermal softening parameter ($\beta = 0.0016$ per $^{\circ}$C) permits a relatively weak imperfection ($f = 0.9994$) to result in localization at $\epsilon_{cr} = 0.217$. The results also illustrate the effect of the interaction of the material properties. For example, whether strain hardening is stabilizing or destabilizing depends on the degree of thermal softening. Furthermore, as strain rates decrease, the effects of thermal softening diminish, and the description of the flow potential surface plays a greater role in the localization process. In the analyses with $\dot{\epsilon}_n = 500$ sec^{-1}, the particular description of the combination of isotropic and kinematic hardening is only a secondary effect, altering the localization strain by no more than twenty percent.

Using physically plausible values for the imperfection amplitude f and the thermal parameter $\bar{\xi}$, the flow localization method yields critical strains which are in very close agreement with the results of the full, two-dimensional finite element calculations of shear banding by LeMonds and Needleman [15]. Our present calculations illustrate that the use of constant values of f and $\bar{\xi}$ result in reasonably accurate critical strain predictions over a fairly broad range of material properties.

ACKNOWLEDGEMENTS

The support of this work through ARO Grant DAAG29-85-K-0003 is gratefully acknowledged. The computations reported on here were carried out at the Brown University, Division of Engineering, Computational Mechanics Facility. The acquisition of this facility was made possible by grants from the U.S. National Science Foundation (Grant ENG78-19378), the General Electric Foundation, the Ford Motor Company and the Digital Equipment Corporation.

REFERENCES

[1] Hill, R., "Acceleration Waves in Solids," *J. Mech. Phys. Solids*, Vol. 13, p. 10-16, 1962.

[2] Thomas, T.Y., Plastic Flow and Fracture in Solids, Academic Press, New York, 1961.

[3] Mandel, J., Rheology and Soil Mechanics, eds. J. Kravtchenko and P.M. Sirieys, Springer-Verlag, 1966.

[4] Rice, J.R., "The Localization of Plastic Deformation," in Theoretical and Applied Mechanics, ed. W.T. Koiter, North-Holland, Amsterdam, pp. 207-220, 1976.

[5] Hill, R. and Hutchinson, J.W., "Bifurcation Phenomena in the Plane Tension Test," *J. Mech. Phys. Solids*, Vol. 23, pp. 239-264, 1975.

[6] Needleman, A. and Rice, J.R., "Limits to Ductility Set by Plastic Flow Localization," in Mechanics of Sheet Metal Forming, eds. D.P. Koistinen and N.M. Wang, Plenum Press, New York, 1978.

[7] Marciniak, Z. and Kuczynski, K., "Limit Strains in the Processes of Stretch-Forming Sheet Metal," *Int. J. Mech. Sci.*, Vol. 9, 1967.

[8] Hutchinson, J.W. and Tvergaard, V., "Shear Band Formation in Plane Strain," *Int. J. Solids Struct.*, Vol. 17, pp. 451-470, 1981.

[9] Saje M., Pan, J. and Needleman A., "Void Nucleation Effects on Shear Localization in Porous Plastic Solids," *Int. J. Fracture*, Vol. 19, pp. 163-182, 1982.

[10] Pan, J., Saje M. and Needleman A., "Localization of Deformation in Rate Sensitive Porous Plastic Solids," *Int. J. Fracture*, Vol. 21, pp. 261-278, 1983.

[11] Rudnicki, J.W. and Rice, J.R., "Conditions for the Localization of Deformation in Pressure-Sensitive Dilatant Materials," *J. Mech. Phys. Solids*, Vol. 23, pp. 371-394, 1970.

[12] Tvergaard, V., "Effect of Kinematic Hardening on Localized Necking in Biaxially Stretched Sheets," *Int. J. Mech. Sci.*, Vol. 20, pp. 651-658, 1978.

[13] Needleman, A. and Tvergaard, V., "Limits to Formability in Rate Sensitive Metal Sheets," in Mechanical Behavior of Materials, eds. J. Carlsson and N.G. Ohlson, Pergammon, pp. 51-65, 1984.

[14] Taylor, G.I. and Quinney, H., "The Latent Energy Remaining in a Metal After Cold Working," *Proc. Roy. Soc. London 143*, 1934.

[15] LeMonds J. and Needleman, A., "Shear Localization in Rate and Temperature Sensitive Materials," to be published.

[16] Staker, M.R., "The Relation Between Adiabatic Shear Instability Strain and Material Properties," *Acta Metall.*, Vol. 32, pp. 683-689, 1981.

[17] Goel, R.P. and Malvern, L.E., "Biaxial Plastic Simple Waves With Combined Kinematic and Isotropic Hardening," *J. Appl. Mech.*, Vol. 37, 1970.

[18] Peirce, D., Shih, C.F., and Needleman, A., "A Tangent Modulus Method for Rate Dependent Solids," *Computers and Structures*, Vol. 18, pp. 875-887, 1984.

[19] Needleman, A., "Finite Elements for Finite Strain Plasticity Problems," in Plasticity of Metals at Finite Strain: Theory, Computation, and Experiment, edited by E.H. Lee and R.H. Mallett, pp. 387-436, Stanford University, 1982.

[20] Hartley, K.A., "Temperature Measurements During the Formation of Shear Bands at High Rates of Deformation," Ph.D. Thesis, Brown University, 1986.

[21] Clifton, R.J., "Adiabatic Shear Banding," Chapter 8 in Materials Response to Ultra High Loading Rates, National Materials Advisory Committee, NMAB-356, 1980.

[22] Rice, J.R. and Tracey, D.M., "On the Ductile Enlargement of Voids in Triaxial Stress Fields," *J. Mech. Phys. Solids*, Vol. 17, pp. 201-217, 1969.

[23] McClintock, F.A., "A Criterion for Ductile Fracture by the Growth of Holes," *J. Appl. Mech.*, Vol. 35, pp. 363-371, 1968.

TABLE 1

Values of the non-dimensional thermal parameter $\bar{\xi}$ in (2.7) which result in localization at the critical strain which marks the point of shear band initiation in the finite element calculations with kinematic hardening presented in [15]. The adiabatic limit is specified by $\bar{\xi} \to 0$ and the uniform temperature limit is given by $\bar{\xi} \to \infty$. The imperfection amplitude is f = 0.9994. The values of all other material properties are specified in the text.

$\dot{\epsilon}_n/\dot{\epsilon}_o$	ϵ_{cr}-FEA	$\bar{\xi}$
5×10^5	0.218	3.37
5×10^4	0.335	11.86
5×10^3	0.537	25.34

TABLE 2

Critical strain predictions of the flow localization method compared with the critical strains at which shear bands were observed initiated in finite element calculations carried out here using the analytical method presented in [15]. The imperfection amplitude is f = 0.9994. The values of all other material properties are specified in the text.

Parameter	Value	$\bar{\xi}$	λ	ϵ_{cr}-FEA	ϵ_{cr}-FLOC
β	0.00105	3.37	0	0.330	0.347
β	0.0020	3.37	0	0.168	0.168
N	0.20	3.37	0	0.295	0.296
N	0.30	3.37	0	0.277	0.286
m	0.025	0	1	0.193	0.200
m	0.002	3.37	0	0.175	0.150
m	0.025	3.37	0	0.283	0.293
η	0.75	3.37	0	0.345	0.359
η	1.50	3.37	0	0.174	0.164

FIGURE CAPTIONS

Fig. 1 The imperfection band (b) and strip of surrounding material (s) separated by the characteristic length ℓ. Plane strain compression occurs in the x^2 direction.

Fig. 2 Localization strain ϵ_{cr} vs. the imperfection amplitude $f = \sigma_o^b/\sigma_o^s$ for an isotropically hardening solid deformed at $\dot{\epsilon}_n/\dot{\epsilon}_o = 5\times10^5$ ($\dot{\epsilon}_n = 500\ sec^{-1}$). The value of the Fourier modulus in (2.7) is $\bar{\xi} = 0$, which corresponds to the adiabatic limit. The values of all other material properties are specified in the text.

Fig. 3 Localization strain ϵ_{cr} vs. the non-dimensional parameter $\bar{\xi}$ in (2.7) for a kinematically hardening solid deformed at $\dot{\epsilon}_n/\dot{\epsilon}_o = 5\times10^5$ ($\dot{\epsilon}_n = 500\ sec^{-1}$), with the imperfection amplitude $f = 0.9994$. The values of all other material properties are specified in the text.

Fig. 4 Localization strain ϵ_{cr} vs. the thermal softening parameter β in (3.5) for a kinematically hardening solid deformed at $\dot{\epsilon}_n/\dot{\epsilon}_o = 5\times10^5$ ($\dot{\epsilon}_n = 500\ sec^{-1}$), with the imperfection amplitude $f = 0.9994$ and $\bar{\xi} = 3.37$ in (2.7). The values of all other material properties are specified in the text. Points labelled with an 'X' correspond to results of finite element calculations.

Fig. 5 Localization strain ϵ_{cr} vs. the strain hardening exponent N in (3.6) for a kinematically hardening solid deformed at $\dot{\epsilon}_n/\dot{\epsilon}_o = 5\times10^5$ ($\dot{\epsilon}_n = 500\ sec^{-1}$), with the imperfection amplitude $f = 0.9994$ and $\bar{\xi} = 3.37$ in (2.7). The values of all other material properties are specified in the text. Points labelled with an 'X' correspond to results of finite element calculations.

Fig. 6 Localization strain ϵ_{cr} vs. the strain rate sensitivity exponent m in (3.5) for a kinematically hardening solid deformed at $\dot{\epsilon}_n/\dot{\epsilon}_o = 5\times10^5$ ($\dot{\epsilon}_n = 500$ sec^{-1}), with the imperfection amplitude f = 0.9994 and $\bar{\xi} = 3.37$ in (2.7). The values of all other material properties are specified in the text. Points labelled with an 'X' correspond to results of finite element calculations.

Fig. 7 Localization strain ϵ_{cr} vs. the non-dimensional parameter η in (2.7), which measures the magnitude of the rate of internal heat generation, for a kinematically hardening solid deformed at $\dot{\epsilon}_n/\dot{\epsilon}_o = 5\times10^5$ ($\dot{\epsilon}_n = 500$ sec^{-1}), with the imperfection amplitude f = 0.9994 and $\bar{\xi} = 3.37$ in (2.7). The values of all other material properties are specified in the text. Points labelled with an 'X' correspond to results of finite element calculations.

Fig. 8 Localization strain ϵ vs. the imperfection plane orientation angle ψ (—— initial angle, - - - angle at localization) for a kinematically hardening solid deformed at $\dot{\epsilon}_n/\dot{\epsilon}_o = 5\times10^5$ ($\dot{\epsilon}_n = 500$ sec^{-1}), with the imperfection amplitude f = 0.9994 and $\bar{\xi} = 3.37$ in (2.7). The values of all other material properties are specified in the text.

Fig. 9 Jump in hydrostatic stress across the imperfection band interface, normalized with respect to σ_o in (3.6), vs. ϵ, the maximum principle logarithmic strain outside the band. The solid hardens kinematically and is deformed at $\dot{\epsilon}_n/\dot{\epsilon}_o = 5\times10^5$ ($\dot{\epsilon}_n = 500$ sec^{-1}), with the imperfection amplitude f = 0.9994 and $\bar{\xi} = 3.37$ in (2.7). The values of all other material properties are specified in the text.

Fig. 10 Localization strain ϵ_{cr} vs. the mixed hardening parameter λ in (3.6) and (3.7) for a solid deformed at $\dot{\epsilon}_n/\dot{\epsilon}_o = 5\times10^3$ ($\dot{\epsilon}_n = 5$ sec^{-1}), with the imperfection amplitude f = 0.9994 and $\bar{\xi} = 25.34$ in (2.7). The values of all other material properties are specified in the text.

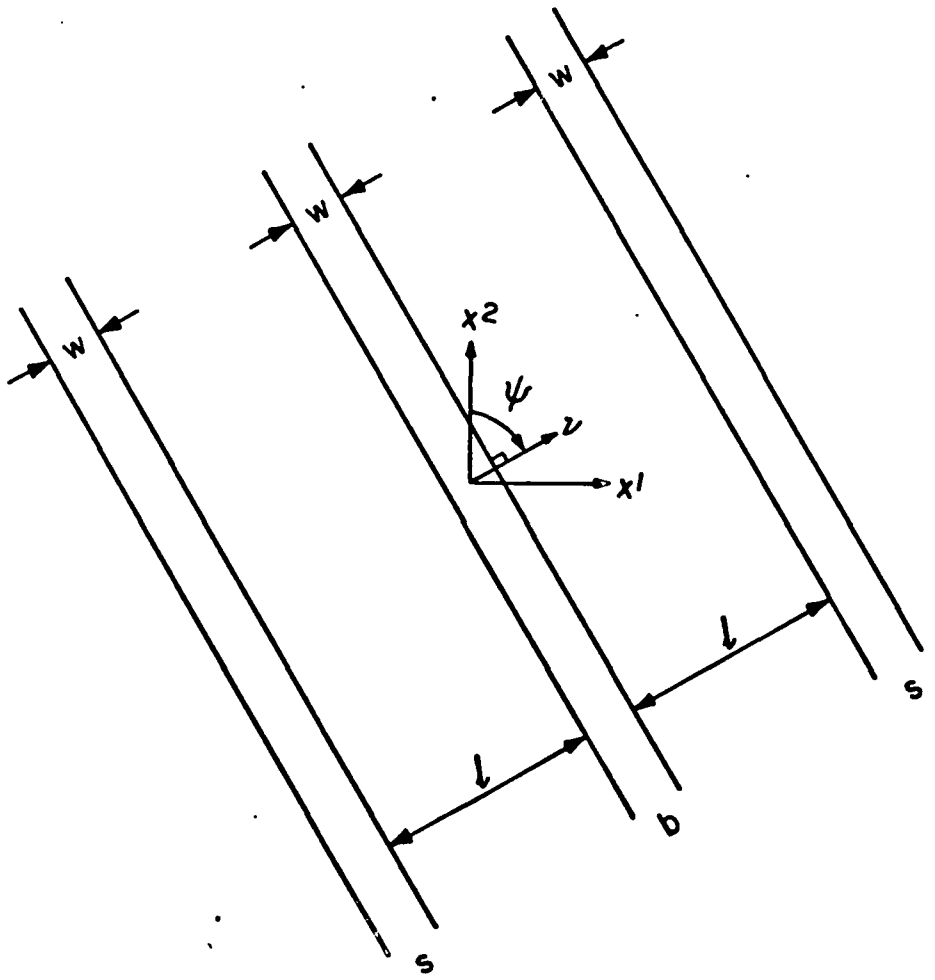

FIGURE 1

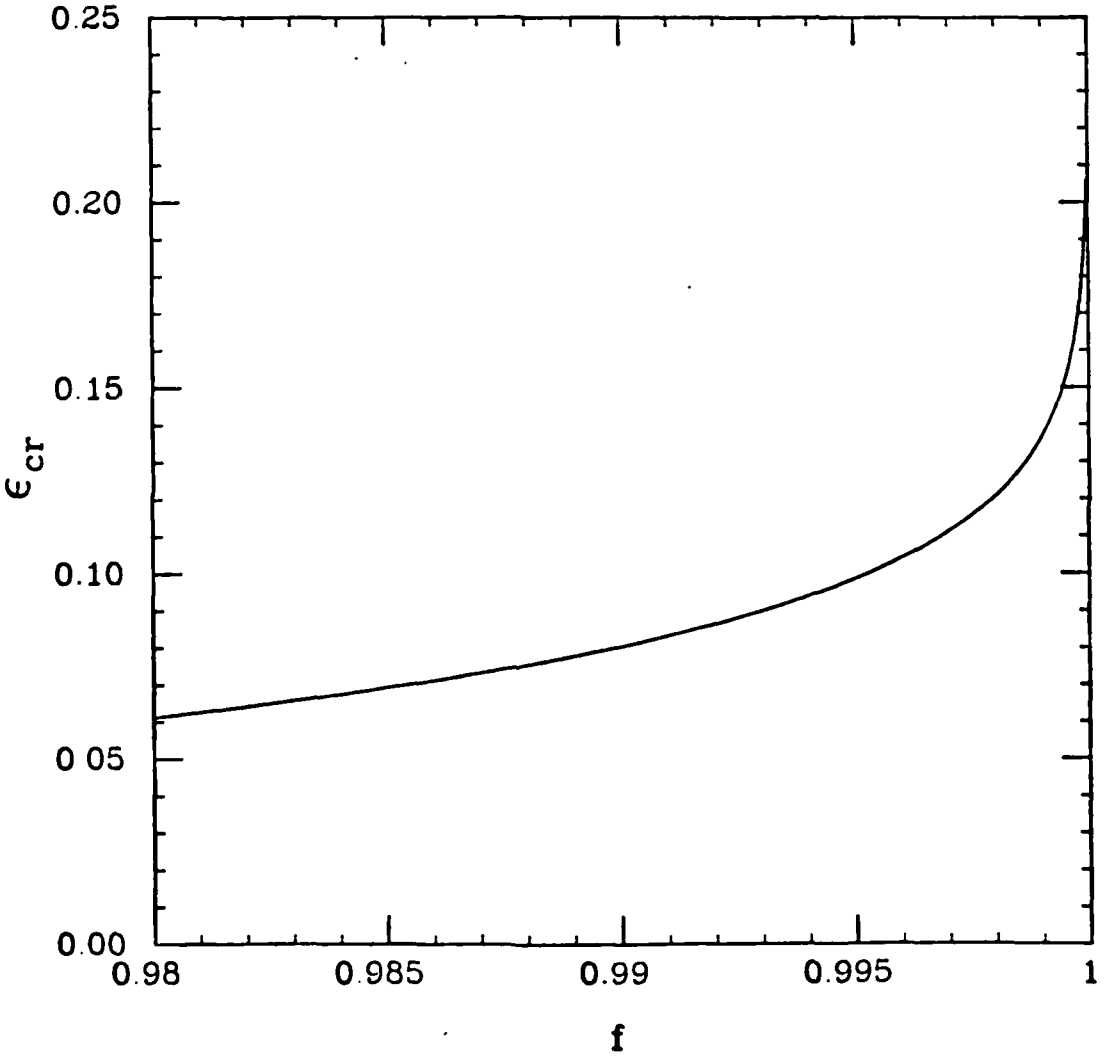

FIGURE 2

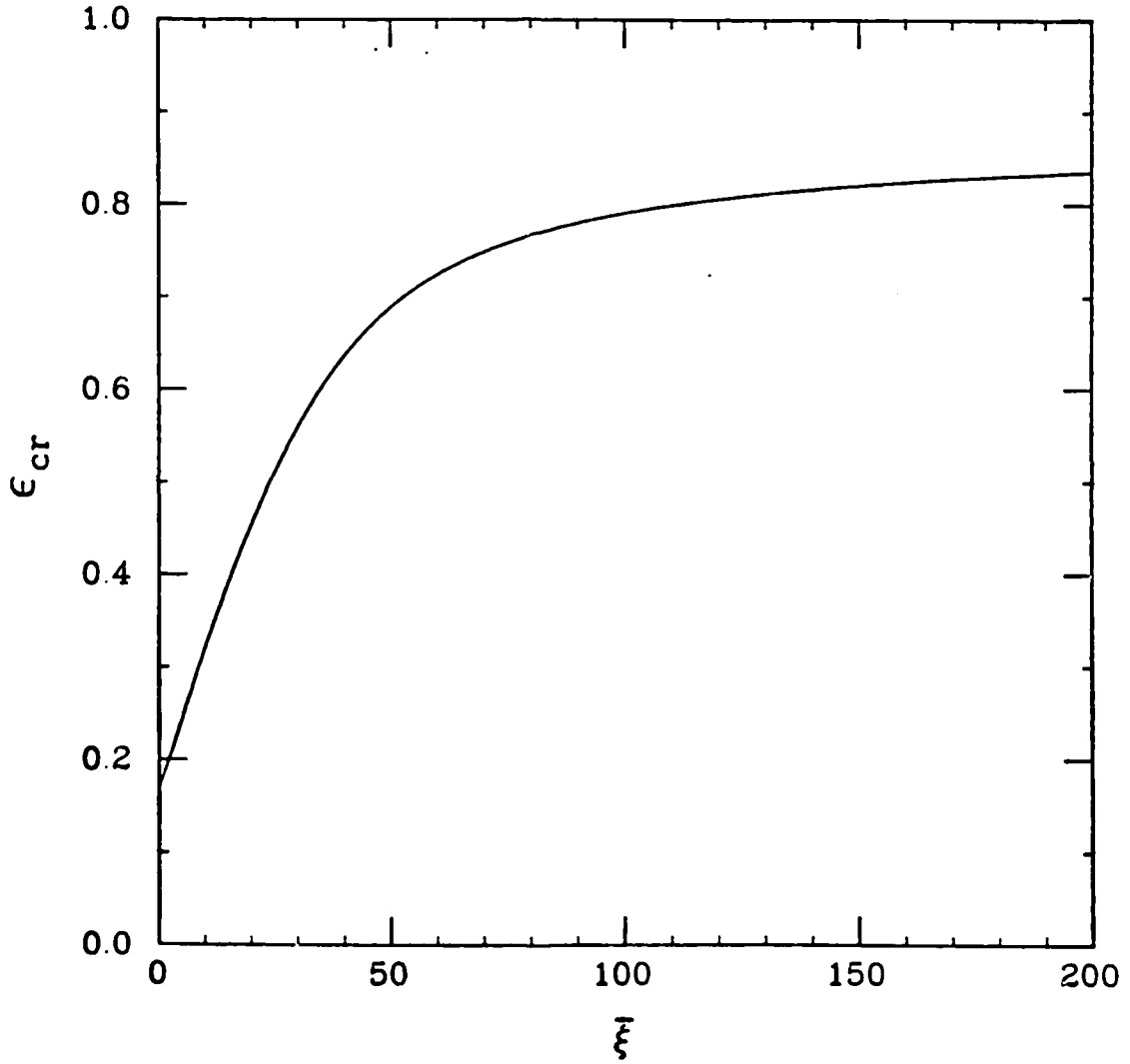

FIGURE 3

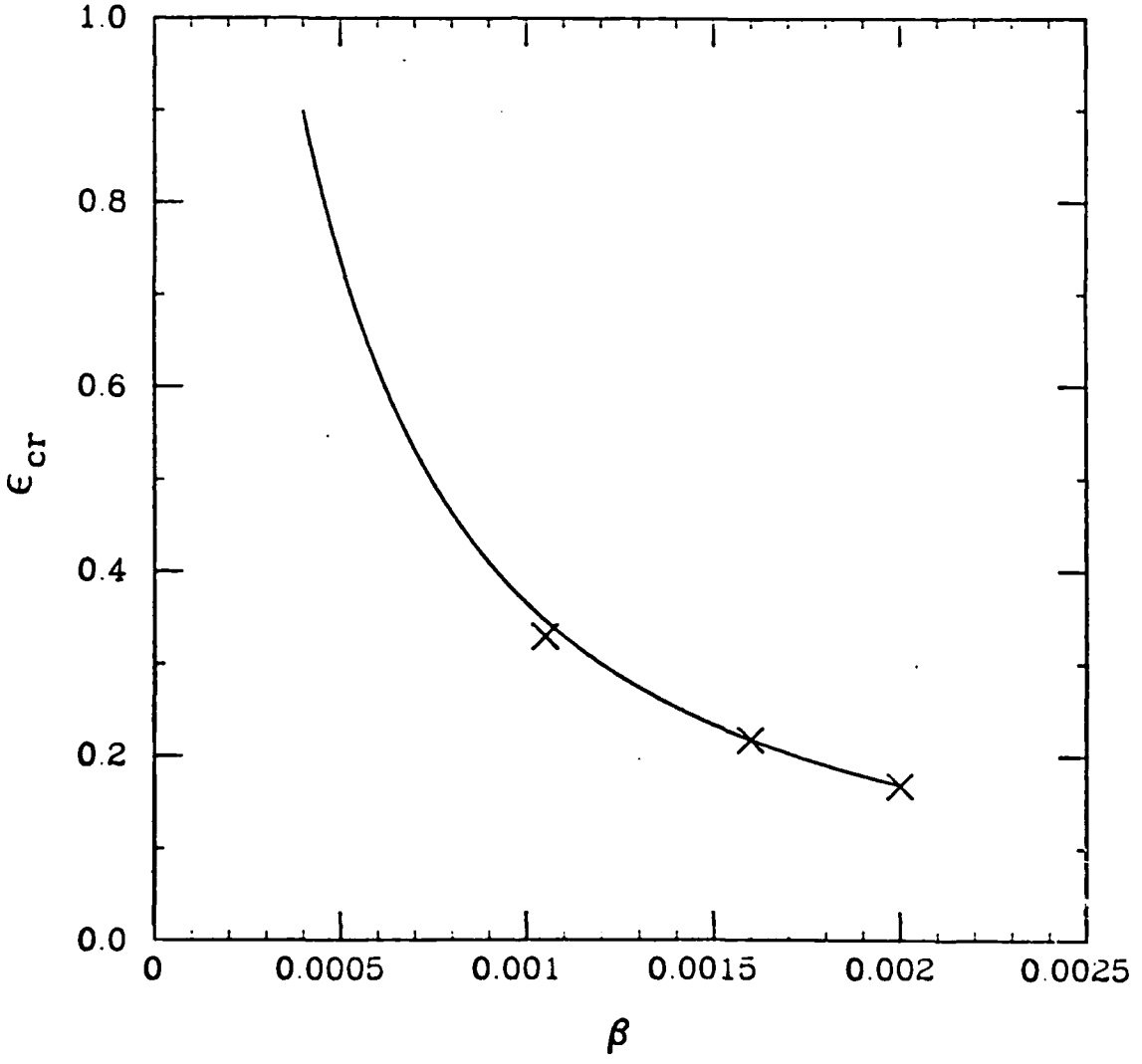

FIGURE 4

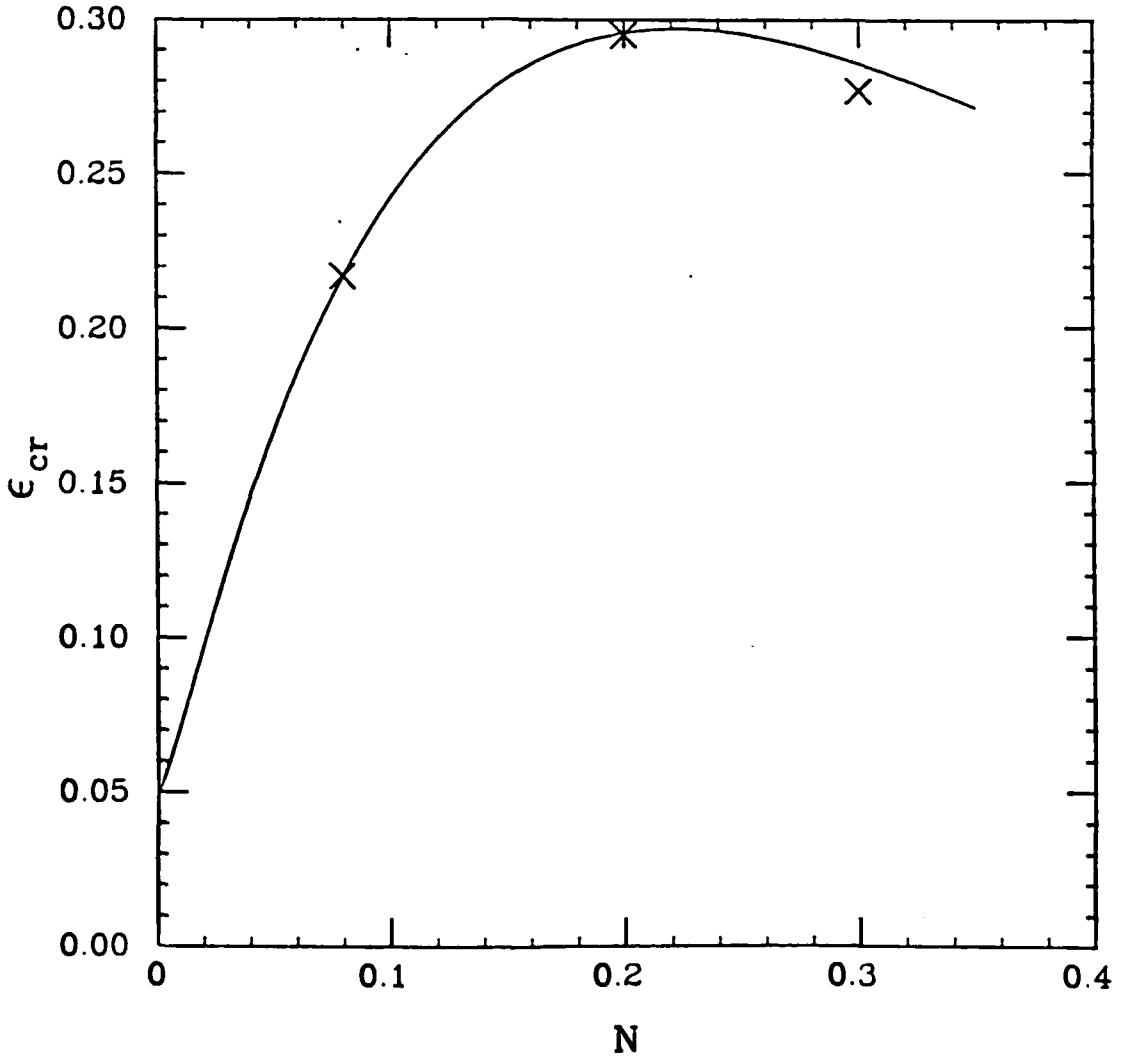

FIGURE 5

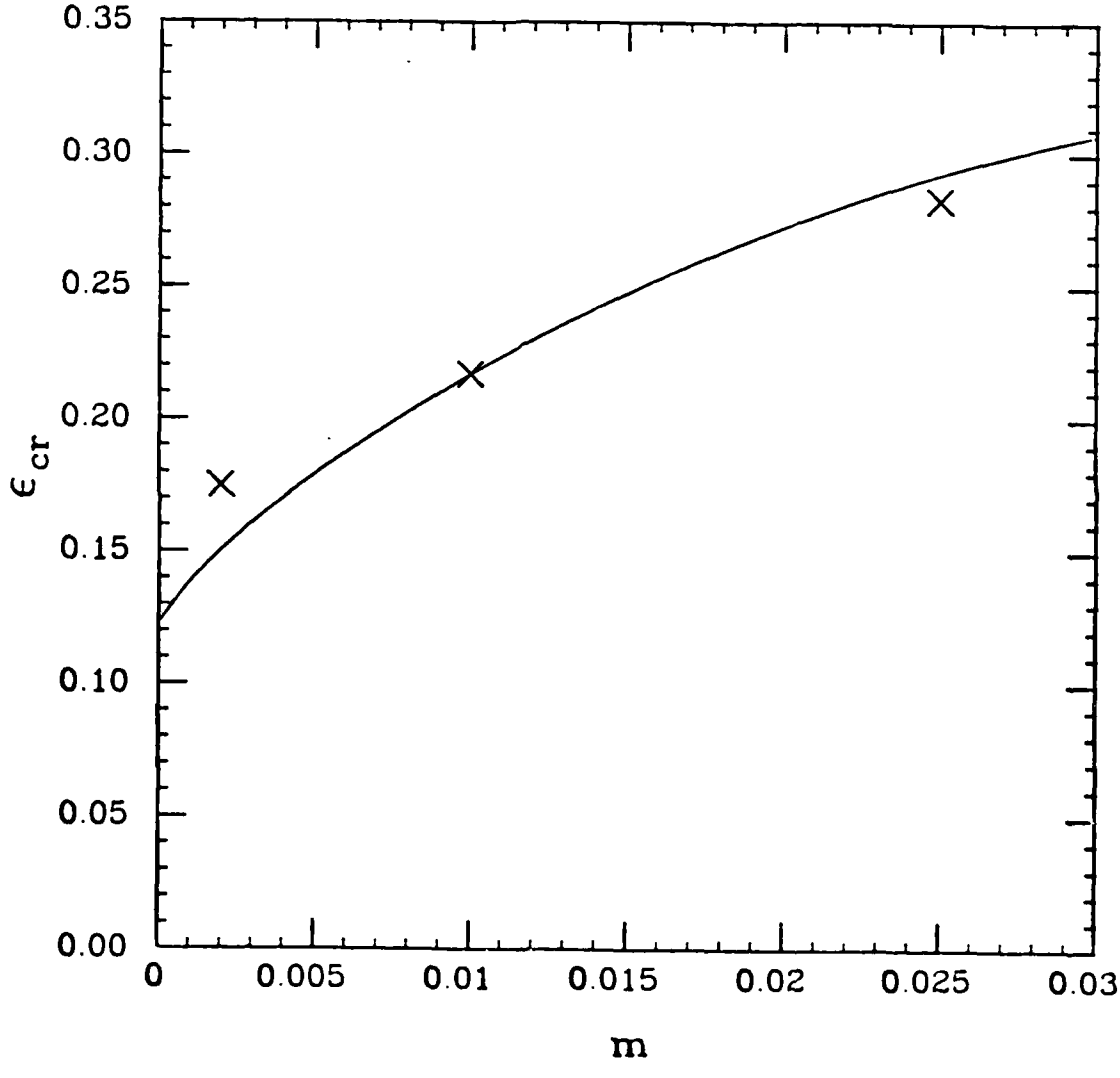
0.35
0.30
0.25
0.20
0.15
0.10
0.05
0.00
ϵ_{cr}
0
0.005
0.01
0.015
0.02
0.025
0.03
m

FIGURE 6

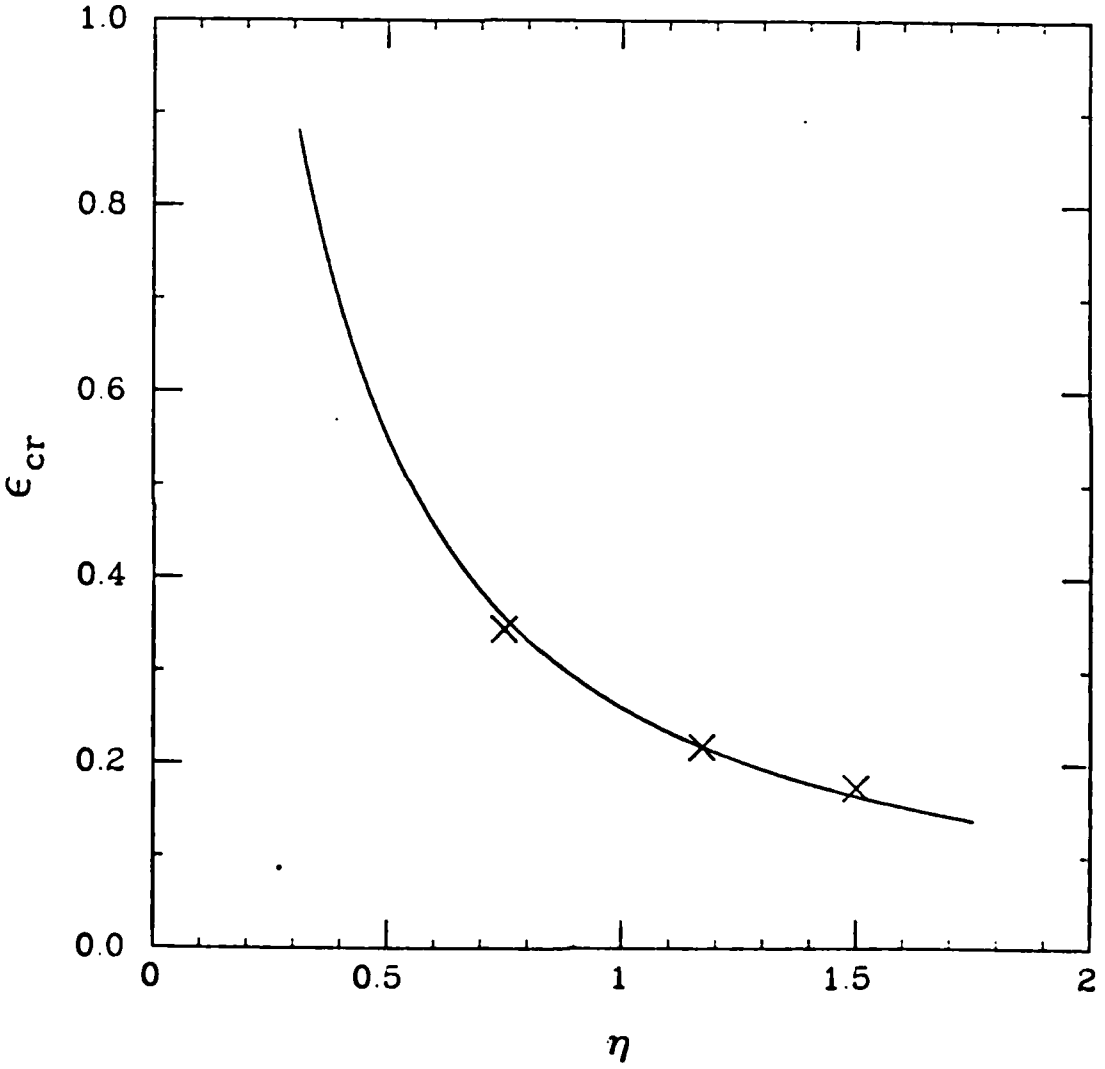

FIGURE 7

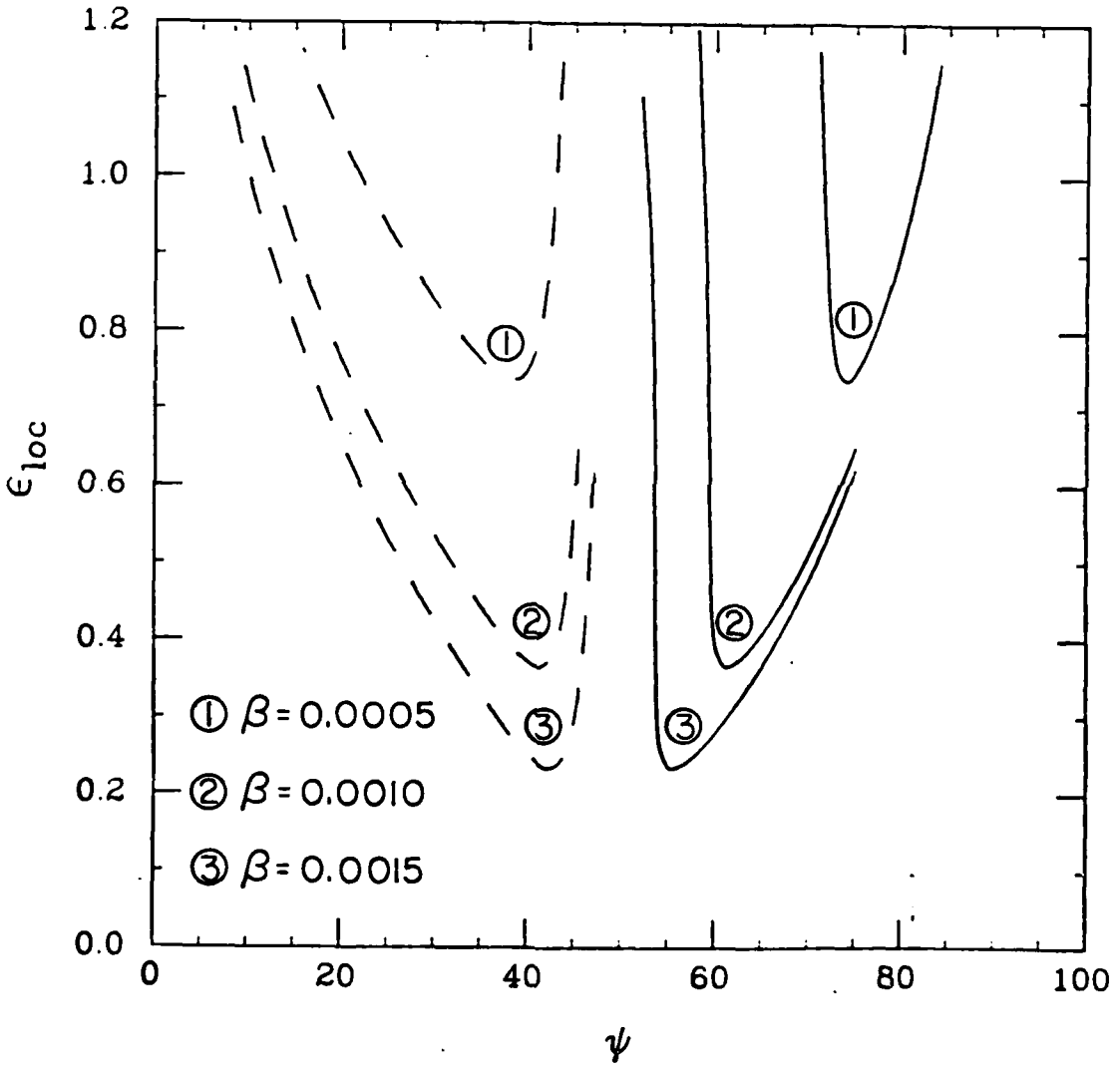
1.2
1.0
0.8
0.6
0.4
0.2
0.0
ϵ_{loc}
0
20
40
60
80
100
ψ
① β = 0.0005
② β = 0.0010
③ β = 0.0015

FIGURE 8

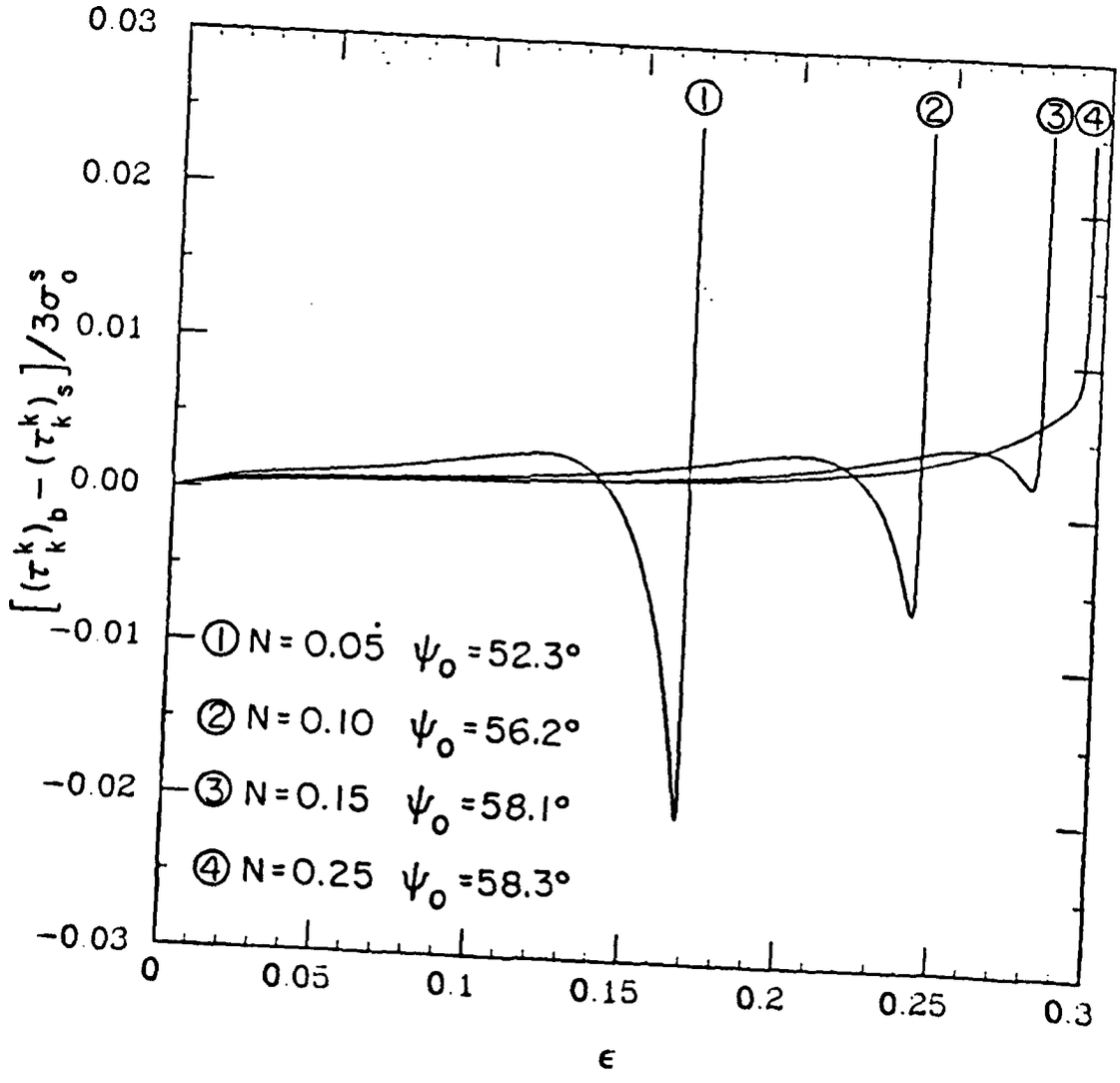
0.03
0.02
0.01
0.00
−0.01
−0.02
−0.03
0
0.05
0.1
0.15
0.2
0.25
0.3
ϵ
$[(\tau^k_k)_b - (\tau^k_k)_s]/3\sigma^s_o$
① N = 0.05 ψ_o = 52.3°
② N = 0.10 ψ_o = 56.2°
③ N = 0.15 ψ_o = 58.1°
④ N = 0.25 ψ_o = 58.3°

FIGURE 9

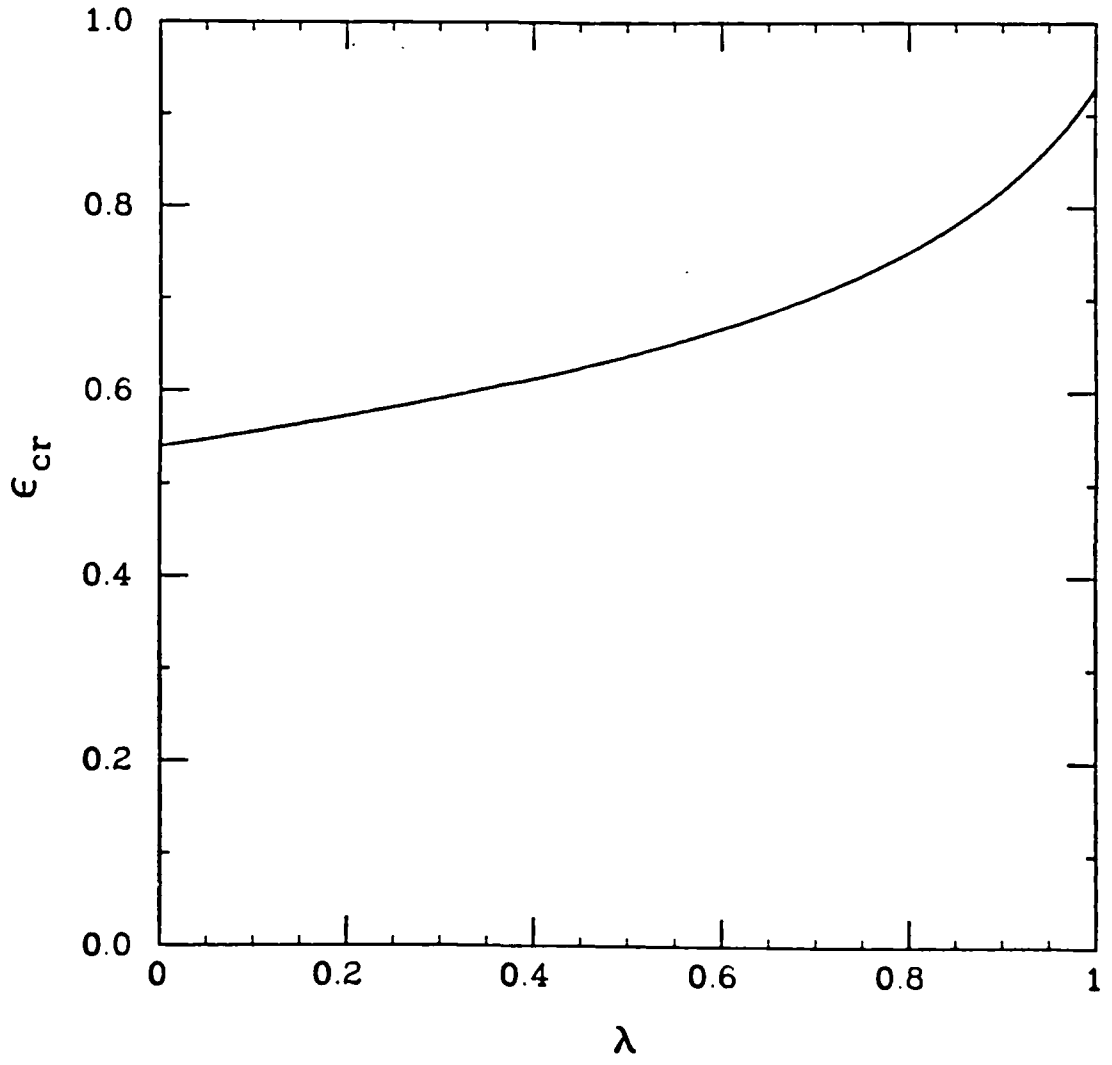

FIGURE 10

END

DTIC

8-86